A SUBSTRATE INTEGRATED WAVEGUIDE TO SUBSTRATE INTEGRATED COAXIAL LINE TRANSITION

Qiang Liu[1], Yuanan Liu[1], Yongle Wu[1, 2, *], Junyu Shen[1], Shulan Li[1], Cuiping Yu[1], and Ming Su[1]

[1]School of Electronic Engineering, Beijing University of Posts and Telecommunications, Beijing, China

[2]State Key Laboratory of Millimeter Waves, Southeast University, Nanjing 210096, China

Abstract—In this paper, a novel substrate integrated waveguide (SIW) to substrate integrated coaxial line (SICL) transition using the 3 dB SIW power divider (PD) and SIW 180° phase shifter (PS) is proposed. The SIW-to-SICL transition realizes the easy integration of SIW, SICL, and active device in the same microwave communication system based on the substrate-integrated technology (SIT). To validate the design concept, the prototype has been fabricated and measured. Measurements are in good agreement with simulations, and shows that the SIW-to-SICL transition features ultra-low insertion loss lower than 0.25 dB and with a fractional bandwidth over 10%.

1. INTRODUCTION

Substrate integrated waveguide (SIW) and substrate integrated coaxial line (SICL) are becoming more and more popular [1, 2], and substrate-integrated technology (SIT) represents an emerging and promising candidate for the development of components and circuits operating in the microwave and millimeter-wave or terahertz region [3–9]. As shown in Fig. 1, SIW structure is fabricated by two rows of metallic via holes in a dielectric substrate, which connect two grounded parallel metal plates, and permit the implementation of conventional metallic rectangular waveguide in planar circuit form [1]. SIW have many advantages, including easy fabrication and low cost compared with conventional metallic rectangular waveguide [3, 4]. The fundamental

mode of the SIW is the dispersion mode TE_{10}, and it is not convenient for integrating with other active devices. As shown in Fig. 2, SICL is a shielded planar coaxial transmission line, comprising a conductive stripline sandwiched between the two grounded dielectric layers and side-limited by two rows of metallic via holes, which is used to keeping it away from lateral leakage, cross-talk and the propagation of the unwanted parallel-plate mode [6]. Because of the no-dispersive fundamental mode TEM, SICL has a broadband of single-mode operation for the design of ultra-wideband and miniaturization microwave components and circuits [7, 8]. Moreover, SICL can enhance the directivity of the couplers without changing the configuration of the coupled-SICL [9]. SIW is a high-pass system for the TE_{10} mode cutoff frequency property. However, SICL is a low-pass system, and the highest frequency of the SICL single-mode operation bandwidth equals the cut-off frequency of the first upper mode TE_{10}, which can be adjusted by changing the distance between two via holes.

At present, many SIW passive components have been studied, such as filters [10–12], power dividers [13], phase shifters [14, 15], diplexers [16], antennas [17, 18], and so on. However, active SIW circuits are hardly ever used. This is mainly due to the difficulties in the integration of the active devices. Transitions from SIW to other quasi-TEM lines are generally used to overcome this problem, and see for instance the oscillator proposed in [19] or
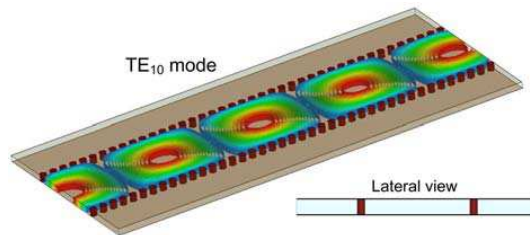
Figure 1. Structures and the fundamental mode TE_{10} of SIW.
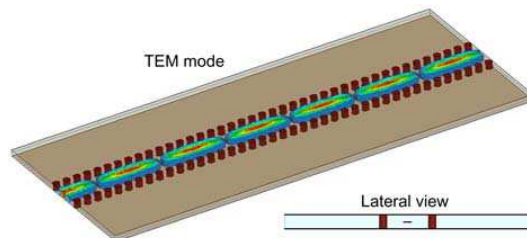
Figure 2. Structures and the fundamental mode TEM of SICL.

the low noise amplifier presented in [4]. Due to the radiation loss, SIW-to-quasi-TEM transmission line transition such as SIW-to-microstrip line (MS) transition [1], SIW-to-coplanar waveguide (CPW) transition [20], and SIW-to-conductor backed coplanar waveguide (CBCPW) transition [21] may damage the signal integrity and produce signal interference in the circuits and systems operating in microwave or millimeter wave bands. The SIW-to-SICL transition combines the advantages of SIW and SICL in one microwave substrate-integrated active or passive circuits and systems at the same time. Moreover, SIW-to-SICL transition is suitable for multilayer circuit structures such as low temperature co-fired ceramic (LTCC). The transition converts the TE_{10} fundamental mode in SIW to TEM fundamental mode in SICL smoothly, and ensures that other unwanted high-order mode is not excited around the discontinuity region at the same time. However, there are *no papers* that report such a transition to the best of our knowledge. In this paper, a novel SIW-to-SICL transition based on the SIW 3 dB power divider (PD) [10] and SIW 180° phase shifter (PS) [15] is proposed. The SIW-to-SICL transition with centre operating frequency of 7 GHz is constructed, fabricated, and measured. The microstrip line to SIW (MS-to-SIW) transition, SICL-to-CBCPW transition [9], and SMA connectors are employed for measurement conveniently. The measurement results and simulation results of the SIW-to-SICL transition are in good agreement and verify our proposed idea. The measured return loss is better than 15 dB and the insertion loss is lower than 0.25 dB from 6.70 to 7.42 GHz with a fractional bandwidth of over 10%. The SIW-to-SICL transition realizes the easy integration of SIW, SICL, and active device in the same microwave communication system based on the SIT.

2. THE DESIGN AND PRINCIPLE OF THE SIW-TO-SICL TRANSITION

Structures of the proposed SIW-to-SICL transition are shown in Fig. 3. The input port of the transition is SIW on the left side, and the distance between its two rows of metallic cylinders is W_1. The output port of the transition is SICL on the right side. The width of the center conductive stripline of the SICL is W_4, and the distance of the side-limited two rows of metallic cylinders is W_5. Seen from Fig. 3(a), the proposed transition is composed of two parts: SIW 3 dB PD and SIW 180° PS. The SIW 3 dB PD locates at cross-sectional BB' marked in Fig. 3(b), consisting of two substrate layers with a conductor plane inserted in the middle of the structure. The SIW 180° PS with length L_0 in the region from the starting point at cross-sectional BB' to the end point
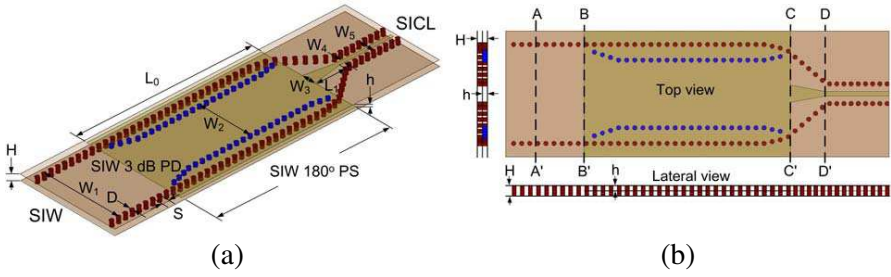
Figure 3. The structures of the proposed SIW-to-SICL transition. (a) The 3D view. (b) The top and the lateral view.
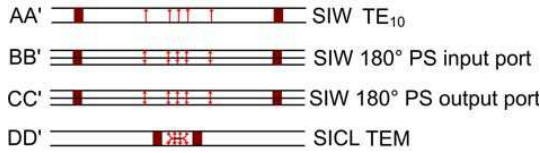
Figure 4. The electric field distributions at the cross sections AA', BB', CC', and DD' marked in Fig. 3(b).

at CC' is composed of the lower and upper SIW with different widths W_1 and W_2, which are separated by the middle metal plane. For the transmission performance enhancement to the transition, the tapered structure with length L_1 in the region from the cross-sectional CC' to the DD' is employed, and this smooth transition ensures the field and impedence matching between SIW 180° PS output port and SICL in the broad bandwidth.

As illustrated in Fig. 3, the SIW-to-SICL transition is implemented in a bilayer dielectric substrate with three metallic layers: top layer, middle layer, and bottom layer. The inner conductor is realized on the middle metallic layer, and the ground is comprised by the top and bottom metallic layers. Each substrate has a same thickness of h, and thickness of the whole converter is $H = 2h$. The diameter of the metallic cylinders is D and the period of the side limited metallic cylinders is S in the propagation direction of the electromagnetic wave.

Figure 4 gives the four cross-sectional views of electric field distributions at AA', BB', CC', and DD' marked in Fig. 3(b) respectively, which demonstrates the operation principle and the conversion process of the proposed SIW-to-SICL transition. Firstly, the electric field in the SIW is TE_{10} mode at AA', which is the fundamental mode of SIW as shown in Fig.1. Secondly, the SIW 3 dB

PD at BB' splits this TE_{10} field into two ways of same-direction SIW TE_{10} field, which excite the upper and lower SIW at SIW 180° PS input port, respectively. Thirdly, SIW 180° PS converts the same-direction fields at BB' into the reverse-direction fields at CC', which have 180 degree phase difference output. After linearly tapered transforming from CC' to DD', the TEM mode is excited at DD' in SICL finally. Seen from the conversion process of the SIW-to-SICL transition in Fig. 4, SIW 3 dB PD and SIW 180° PS are the key components in it.

If the SIW 180° PS length L_0 satisfies the equation of

$$\Delta\varphi = [\beta_1(W_1) - \beta_2(W_2)] \cdot L_0 = \pi \tag{1}$$

the phase difference of π between the fields in the upper and lower parts of the SIW 180° PS output can be obtained, and achieve the reverse-direction fields at CC' as shown in Fig. 4. In (1), $\beta_1(W_1)$ and $\beta_2(W_2)$ are the propagation constants of the TE_{10} mode in the lower and upper SIW, which width are W_1 and W_2, respectively.

The fundamental mode of the SIW is TE_{10} mode, and the dispersion characteristics are equivalent to those of a related rectangular waveguide with an equivalent width. We assume that the width between the two rows of metallic cylinders of the SIW is W, the diameter of metalized via hole is D, and the space between adjacent via hole is S. The equivalent width of the SIW is written as follows [22]:

$$W_{eff} = W - 1.08 \cdot \frac{D^2}{S} + 0.1 \cdot \frac{D^2}{W} \tag{2}$$

Therefore, the propagation constant of the SIW can written as

$$\beta(W) = \sqrt{\omega^2 \mu \varepsilon - \left(\frac{\pi}{W_{eff}}\right)^2} \tag{3}$$

From (2) and (3), the propagation constant β is determined by the width W of SIW completely for given D, S, ω, ε, and μ. The propagation constant β of SIWs with different width W are shown in Fig. 5, which are obtained with the aid of Ansys High Frequency Structural Simulator (HFSS) 14.0.

Similar to the conventional metallic rectangular waveguide, SIW has cut-off frequency for the fundamental mode TE_{10} as follows:

$$f_{\mathrm{TE}_{10}} = \frac{c}{2W_{eff} \cdot \sqrt{\varepsilon_r}} \tag{4}$$

where ε_r is the relative dielectric permittivity and c the light speed. The selection of the operation frequency bandwidth should keep the SIW operating in the fundamental mode TE_{10}. In other words, the operation frequency of the SIW must satisfy the condition: $f_{\mathrm{TE}_{10}} <$
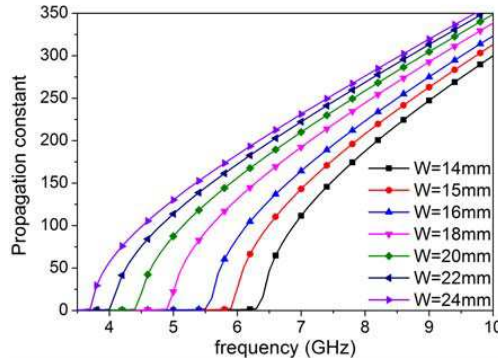
Figure 5. The propagation constant β of SIWs with different width.
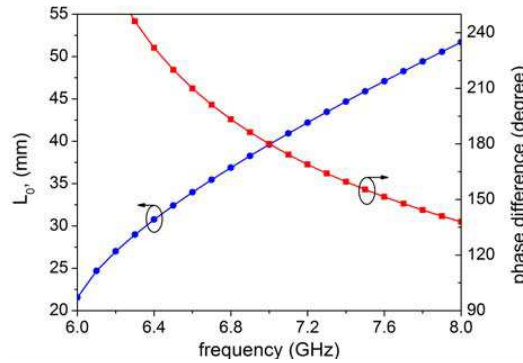
Figure 6. The length L_0 and the phase difference of the SIW 180°
PS.

$f < f_{\mathrm{TE}_{20}}$, and $f_{\mathrm{TE}_{20}}$ is the cut-off frequency of the first high-order
mode TE$_{20}$ as follows:

$$f_{\mathrm{TE}_{20}} = \frac{c}{W_{eff} \cdot \sqrt{\varepsilon_r}} \tag{5}$$

As a special case, the centre operation frequency is set to be 7 GHz.
The width of the lower and upper parts of the SIW 180° PS are chosen
as $W_1 = 22$ mm and $W_2 = 15$ mm, and the relationship between the
length L_0 and the frequency for the condition: $\Delta\varphi = \pi$ in (1) is shown
in Fig. 6. The length L_0 of the SIW 180° PS equals 39.6 mm for
the centre frequency of 7 GHz, and the phase difference $\Delta\varphi$ decreases
against the frequency increasing is given in Fig. 6, too.
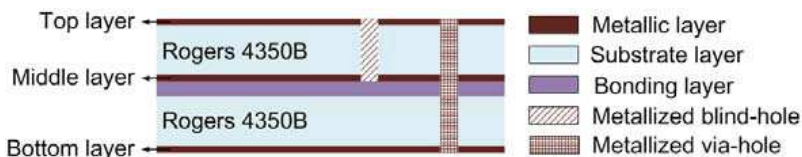
Figure 7. The lateral view of the multilayer board structure.

Table 1. Design parameters of the SIW-to-SICL transition (unit: mm).

Dimensions	W_1	W_2	W_3	W_4	W_5	W_6	W_7	W_8	W_9
Values	22	15	3.8	0.9	4.4	3.6	10	3.4	2.5
Dimensions	L_0	L_1	L_2	L_3	D	D_0	S	G	
Values	46	7.6	10.2	16.2	1	0.9	1.8	0.6	

3. FABRICATED SIW-TO-SICL TRANSITION AND MEASUREMENT

To validate the concept of the design, a prototype of the SIW-to-SICL transition was designed at the centre frequency of 7 GHz. In the design, both the top and bottom dielectric layers are Rogers 4350B with a dielectric constant of 3.48 and a loss tangent of 0.0037. The thickness of each substrate has a thickness of $h = 0.762$ mm and each metallic layer has a thickness of 0.035 mm. A 0.102 mm thick sheet with a dielectric constant of 3.48 and a loss tangent of 0.004 is used for bonding the top and bottom dielectric layers. The thickness H of the fabricated SIW-to-SICL transition is $H = 1.7$ mm approximately and the lateral view of the multilayer board structure is shown in Fig. 7.

The SIW-to-SICL transition was simulated and optimized with the aid of HFSS 14.0. The 3D view and the layouts of the proposed SIW-to-SICL transition are shown in Fig. 8, and the final optimized dimensions of the transition are listed in Table 1. It should be mentioned that the optimized length $L_0 = 46$ mm of the SIW 180° PS is longer than the length $L_0 = 39.6$ mm has designed in Section 2. The employed width between the two rows of metallic cylinders tapered structure in the SIW 180° PS led to this deviation. For measured conveniently, the MS-to-SIW transition and SICL-to-CBCPW transition are employed. The photograph of the fabricated transition is given in Fig. 9, and the S-parameters were measured by an Agilent vector network analyzer 5230C.

The simulation and measurement S-parameters of the fabricated

(a)   (b)
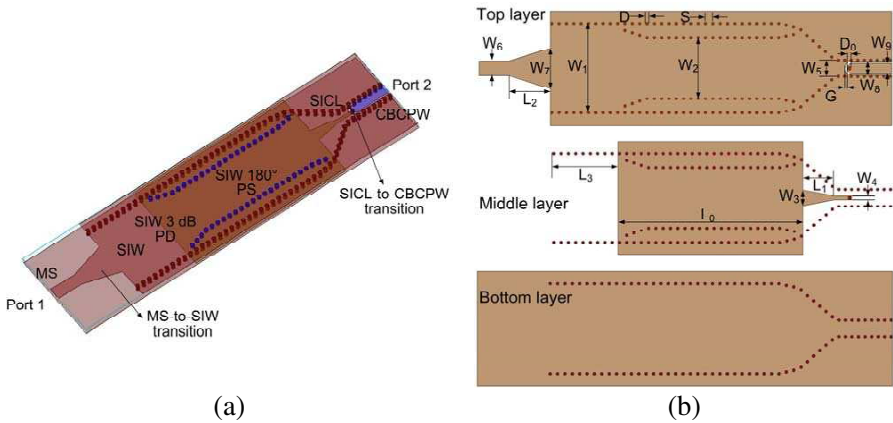
Figure 8. The structures of the SIW-to-SICL transition. (a) The 3D view. (b) The layouts.
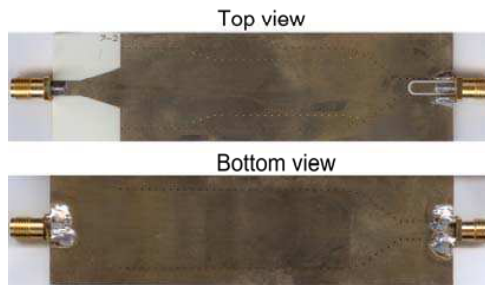
Figure 9. The photograph of the fabricated SIW-to-SICL transition.

transition are shown in Fig. 10, and we can observe the good performance of the transition. The measured return loss ($|S_{11}|$) is better than 15 dB and insertion loss ($|S_{21}|$) of the transition lower than 1.4 dB, from 6.70 to 7.42 GHz with a fractional bandwidth of over 10%. The measurement and simulation results fit very well except that the measured insertion loss $|S_{21}|$ displays between 0.3 and 0.65 dB of extra loss compared with the simulated insertion loss in band in Fig. 10. The extra insertion loss was caused by the two SMA connectors, which was employed in the measurement but not considered in the simulation. It can be obtained that the insertion loss of the SICL-to-SIW transition is lower than 0.25 dB in the passband, in view of the insertion loss caused by the parts of each SAM connector, MS-to-SIW transition and SICL-to-CBCPW transition are 0.3 dB, 0.3 dB, and 0.25 dB at the centre frequency 7 GHz we are measured, respectively.
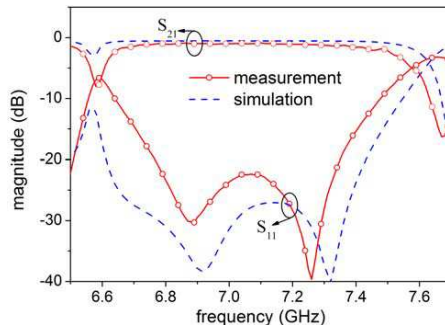
Figure 10. Measured and simulated S-parameters of the fabricated transition.

4. CONCLUSIONS

In this paper, the SIW-to-SICL transition using the 3 dB SIW PD and SIW 180° PS is proposed, designed, and fabricated. The prototype has been fabricated on a bilayer PCB substrate. The measurement and simulation results are in good agreement, and validate the concept of the transition design. The measured return loss is better than 15 dB and insertion loss lower than 0.25 dB, from 6.70 to 7.42 GHz with a bandwidth of over 10%. This design enhances the compatibility of SIW and SICL in the microwave communication system based on SIT. Moreover, the transition reduces the integration difficulty between SIW and active devices. Therefore, such a transition is an excellent candidate in the development of passive or active microwave and millimeter-wave integrated circuits. Further work can be implemented along the wideband and ultra-wideband SIW-to-SICL transition.

ACKNOWLEDGMENT

REFERENCES

1. Deslandes, D. and K. Wu, "Integrated microstrip and rectangular waveguide in planar form," *IEEE Microw. Wireless Compon. Lett.*, Vol. 11, No. 2, 68–70, 2001.

2. Gatti, F., M. Bozzi, L. Perregrini, K. Wu, and R. G. Bosisio, "A novel substrate integrated coaxial line (SICL) for wide-band applications," *36th European Microwave Conference*, 1614–1617, 2006.

3. Bozzi, M., A. Georgiadis, and K. Wu, "Review of substrate-integrated waveguide circuits and antennas," *IET Microwaves, Antennas & Propagation*, Vol. 5, No. 8, 909–920, 2011.

4. He, F. F., K. Wu, W. Hong, L. Han, and X.-P. Chen, "Low-cost 60-GHz smart antenna receiver subsystem based on substrate integrated waveguide technology," *IEEE Trans. Microw. Theory Tech.*, Vol. 60, No. 4, 1156–1165, 2012.

5. Zhou, Y. and S. Lucyszyn, "Modelling of reconfigurable terahertz integrated architecture (Retina) SIW structures," *Progress In Electromagnetics Research*, Vol. 105, 71–92, 2010.

6. Gatti, F., M. Bozzi, L. Perregrini, K. Wu, and R. G. Bosisio, "A new wide-band six-port junction based on substrate integrated coaxial line (SICL) technology," *IEEE Mediterranean Electrotechnical Conference*, 367–370, 2006.

7. Zhu, F., W. Hong, J.-X. Chen, and K. Wu, "Ultra-wideband single and dual baluns based on substrate integrated coaxial line technology," *IEEE Trans. Microw. Theory Tech.*, Vol. 60, No. 10, 3062–3070, 2012.

8. Liang, W. and W. Hong, "Substrate integrated coaxial line 3 dB coupler," *Electronics Letters*, Vol. 48, No. 1, 35–36, 2012.

9. Liu, Q., Y. Liu, Y. Wu, S. Li, C. Yu, and M. Su, "Broadband substrate integrated coaxial line to CBCPW transition for rat-race couplers and dual-band couplers design," *Progress In Electromagnetics Research C*, Vol. 35, 147–159, 2013.

10. Hui, J. N., W. J. Feng, and W. Q. Che, "Balun bandpass filter based on multilayer substrate integrated waveguide power divider," *Electronics Letters*, Vol. 48, No. 10, 571–573, 2012.

11. Xu, Z. Q., Y. Shi, P. Wang, J. X. Liao, and X. B. Wei, "Substrate integrated waveguide (SIW) filter with hexagonal resonator," *Journal of Electromagnetic Waves and Applications*, Vol. 26, Nos. 11–12, 1521–1527, 2012.

12. Gong, K., W. Hong, Y. Zhang, P. Chen, and C. J. You, "Substrate integrated waveguide quasi-elliptic filters with controllable electric

and magnetic mixed coupling," *IEEE Trans. Microw. Theory Tech.*, Vol. 60, No. 10, 3071–3078, 2012.

13. Zou, X., C. M. Tong, and D. W. Yu, "Y-junction power divider based on substrate integrated waveguide," *Electronics Letters*, Vol. 47, No. 25, 1375–1376, 2011.

14. Che, W., E. K.-N. Yung, K. Wu, and X. Nie, "Design investigation on millimeter-wave ferrite phase shifter in substrate integrated waveguide," *Progress In Electromagnetics Research*, Vol. 45, 263–275, 2004.

15. Cheng, Y. J., W. Hong, and K. Wu, "Broadband self-compensating phase shifter combining delay line and equal-length unequal-width phaser," *IEEE Trans. Microw. Theory Tech.*, Vol. 58, No. 1, 203–210, 2010.

16. Han, S., X. L. Wang, Y. Fan, Z. Yang, and Z. He, "The generalized chebyshev substrate integrated waveguide diplexer," *Progress In Electromagnetics Research*, Vol. 73, 29–38, 2007.

17. Cheng, Y. J., "Substrate integrated waveguide frequency-agile slot antenna and its multibeam application," *Progress In Electromagnetics Research*, Vol. 130, 153–168, 2012.

18. Bakhtafrooz, A., A. Borji, D. Busuioc, and S. Safavi-Naeini, "Novel two-layer millimeter-wave slot array antennas based on substrate integrated waveguides," *Progress In Electromagnetics Research*, Vol. 109, 475–491, 2010.

19. Liu, Y., X. H. Tang, and T. Wu, "SIW-based low phase-noise millimeter-wave planar dual-port voltage-controlled oscillator," *Journal of Electromagnetic Waves and Applications*, Vol. 26, Nos. 8–9, 1059–1069, 2012.

20. Lee, S., S. Jung, and H. Y. Lee, "Ultra-wideband CPW-to-substrate integrated waveguide transition using an elevated-CPW section," *IEEE Microw. Wireless Compon. Lett.*, Vol. 18, 746–748, 2008.

21. Deslandes, D. and K. Wu, "Analysis and design of current probe transition from grounded coplanar to substrate integrated rectangular waveguides," *IEEE Trans. Microw. Theory Tech.*, Vol. 53, 2487–2494, 2005.

22. Salehi, M. and E. Mehrshahi, "A closed-form formula for dispersion characteristics of fundamental SIW mode," *IEEE Microw. Wireless Compon. Lett.*, Vol. 21, No. 1, 4–6, 2011.